Spinodal decomposition of off-critical quenches with a viscous phase using dissipative particle dynamics in two and three spatial dimensions

Keir E. Novik*

Cavendish Laboratory, University of Cambridge, Madingley Road, Cambridge CB3 0HE, United Kingdom

Peter V. Coveney[†]

Centre for Computational Science, Department of Chemistry, Queen Mary and Westfield College, University of London, Mile End Road, London E1 4NS, United Kingdom

We investigate the domain growth and phase separation of hydrodynamically correct binary immiscible fluids of differing viscosity as a function of minority phase concentration in both two and three spatial dimensions using dissipative particle dynamics. We also examine the behavior of equal-viscosity fluids and compare our results to similar lattice-gas simulations in two dimensions.

PACS number(s): 64.75.+g, 02.70.−c, 51.10.+y

I. INTRODUCTION

Over the past few years, the dissipative particle dynamics (DPD) model of complex fluids has received considerable attention. It has matured from its somewhat arbitrary initial formulation into a model with a solid theoretical basis. Furthermore, it has been applied with considerable success to a large number of computer simulations of complex fluid systems such as colloidal suspensions, polymeric fluids, spinodal decomposition of binary immiscible fluids, and amphiphilic fluids. DPD also looks promising for simulating multiphase flows and flow in porous media, and is now considered a useful technique alongside the other complex fluid algorithms: molecular dynamics, lattice-gas automata, and techniques based on the lattice-Boltzmann equation. No single technique can yet be applied to all situations, and each has different strengths and weaknesses. While molecular dynamics is in principle the most accurate microscopic approach, in practice it is too slow in both its quantum (Car-Parinello) and classical forms because of its excessive detail. Discrete mesoscopic methods developed from lattice-gas automata have had some success, but they too have problems, such as lacking Galilean invariance. The traditional approach of continuum fluid dynamics has met with limited success in modeling behavior on the length and time scales characteristic of complex fluids.

In this paper we investigate phase separation from both symmetric (critical) and off-critical quenches in binary immiscible fluids of generally differing viscosity using the hydrodynamically correct DPD model. Our motivation is to probe and extend knowledge of the behavior of differing-viscosity fluids, of application, for example, to the action of detergents and the extraction of oil from reservoir rocks.

Phase separation in *equal-viscosity* binary immiscible fluid systems has been simulated using a variety of techniques, including DPD [1–5], molecular dynamics [6–9], Monte Carlo [6,10], cell dynamical systems without hydrodynamics [11] and with Oseen tensor hydrodynamics [12], time-dependent Ginzburg-Landau models with [13–17] and without hydrodynamics [17–19], lattice-gas automata [20–27], and lattice-Boltzmann techniques [28–34]. Spinodal decomposition of *differing-viscosity* immiscible fluids has previously been simulated in two dimensions by a time-dependent Ginzburg-Landau model without hydrodynamics [35]. We discuss the effect of the proportion of each phase on the scaling behavior in both two and three spatial dimensions. We also examine the behavior of equal-viscosity fluids, comparing our results to similar lattice-gas simulations in two dimensions [27].

After describing our fluid model in the following section, we discuss the expected temporal development of the characteristic size of the separating domains in Sec. III. We then describe our method for calculating the characteristic domain size and its rate of growth in Sec. IV. This is followed in Secs. V and VI by information on the simulations performed and a discussion of the results, and by some conclusions in Sec. VII. Finally, as an Appendix to this paper, we make a few comments on the high-performance computing aspects of this work.

II. THE FLUID MODEL

In 1992, Hoogerbrugge and Koelman proposed dissipative particle dynamics [36] as a novel particulate model for the simulation of complex fluid behavior. DPD was developed in an attempt to capture the best aspects of molecular-dynamics and lattice-gas automata. It avoids the lattice-based problems of lattice-gas automata, yet maintains an elegant simplicity and larger scale that keeps the model much faster than molecular dynamics. This simplicity also makes DPD highly extensible, such as for including the interactions of complex molecules or modeling flow in an arbitrary number of spatial dimensions. The key features of the model are that the fluid is grouped into packets, termed ''particles,'' and

---

*Present address: Center for Computational Science, Department of Chemistry, Queen Mary and Westfield College, University of London, Mile End Road, London E1 4NS, United Kingdom. Electronic address: K.E.Novik@qmw.ac.uk

[†]Electronic address: P.V.Coveney@qmw.ac.uk

that mass and momentum are conserved but energy is not. Particles are normally interpreted as representing a coarse-graining of the fluid, so that each particle contains many molecules [36–39]. Since the intrinsic time scale of DPD represents the correlated motion of mesoscopic packets of atoms or molecules, it is typically orders of magnitude larger than the time scale of molecular dynamics [40]. Particle positions and momenta are real variables, and are not restricted to a grid.

Español and Warren's analysis [37] showed that the original DPD model does not satisfy detailed balance, so the equilibrium states (if they exist) cannot be simply characterized. Detailed balance is the condition equating the rates of forward and backward transition probabilities in a dynamical system, and is a sufficient (but not necessary) condition guaranteeing that the system has a (Gibbsian) equilibrium state [41,42]. Español and Warren formulated a Fokker-Planck equation and an equivalent set of stochastic differential equations which lead to an analogous continuous-time model,

$$d\mathbf{p}_i = \sum_{j \neq i} \mathbf{F}_{ij} \, dt = \sum_{j \neq i} [\mathbf{F}_{ij}^C \, dt + \mathbf{F}_{ij}^D \, dt + \mathbf{F}_{ij}^R \, dW_{ij}],$$

$$(1)$$

$$d\mathbf{x}_i = \frac{\mathbf{p}_i}{m_i} dt.$$

In these equations, $\mathbf{p}_i$, $\mathbf{x}_i$, and m_i denote the momentum, position, and mass of particle i. $\mathbf{F}_{ij}^C$ is a conservative force acting between particles i and j, while $\mathbf{F}_{ij}^D$ and $\mathbf{F}_{ij}^R$ are the dissipative and random forces. $dW_{ij} = dW_{ji}$ are independent increments of a Wiener process. By Itô calculus

$$dW_{ij} \, dW_{kl} = (\delta_{ik} \delta_{jl} + \delta_{il} \delta_{jk}) dt,$$

$$(2)$$

so dW_{ij} is an infinitesimal of order $\frac{1}{2}$ and dW_{ij} can be written $\theta_{ij} \sqrt{dt}$, where $\theta_{ij} = \theta_{ji}$ is a random variable with zero mean and unit variance [41]. Detailed balance is satisfied by this continuous-time version of DPD with an appropriate choice for the form of the forces [43], and so equilibrium states are guaranteed to exist and be Gibbsian. To ensure that the associated fluctuation-dissipation theorem holds, Español and Warren suggested the forces assume the following forms [37]:

$$\mathbf{F}_{ij}^C = \alpha \omega_{ij} \hat{\mathbf{e}}_{ij},$$

$$(3)$$

$$\mathbf{F}_{ij}^D = -\gamma \omega_{ij}^2 (\hat{\mathbf{e}}_{ij} \cdot \mathbf{v}_{ij}) \hat{\mathbf{e}}_{ij},$$

$$(4)$$

and

$$\mathbf{F}_{ij}^R = \sigma \omega_{ij} \hat{\mathbf{e}}_{ij},$$

$$(5)$$

where $\mathbf{v}_{ij} = (\mathbf{p}_i/m_i) - (\mathbf{p}_j/m_j)$ is the difference in velocities of particles j and i, $\hat{\mathbf{e}}_{ij}$ is the unit vector pointing from particle j to particle i, and ω_{ij} is a weighting function depending only on the distance separating particles i and j. The constants α, γ, and σ are chosen to reflect the relative importance of the conservative, dissipative (viscous), and random components in the fluid of interest. As a consequence of

detailed balance and the fluctuation-dissipation theorem, γ and σ are related to Boltzmann's constant k_B and the equilibrium temperature T by

$$\frac{\sigma^2}{\gamma} = 2k_B T.$$

$$(6)$$

In order to remain as close as possible to the original DPD model, Español and Warren chose the friction weight function to be

$$\omega_{ij} = 1 - \frac{r_{ij}}{r_c}$$

$$(7)$$

within the constant cutoff length $r_c > 0$ and zero otherwise, where r_{ij} is the distance between particles i and j. Adding Eqs. (3)–(5) together, the total force is

$$\mathbf{F}_{ij} = \left[\alpha - \gamma \omega_{ij} (\hat{\mathbf{e}}_{ij} \cdot \mathbf{v}_{ij}) + \frac{\sigma \theta_{ij}}{\sqrt{dt}} \right] \omega_{ij} \hat{\mathbf{e}}_{ij}.$$

$$(8)$$

Immiscible fluid mixtures exist because individual molecules attract similar and repel dissimilar molecules. The most common example of such behavior arises in mixtures of oil and water below a critical temperature. The nonpolar, hydrophobic molecules of oil attract one another through short-range van der Waals forces, while the polar water molecules have complex, long-range hydrophilic attractions which are dominated by electrostatic interactions, including hydrogen bonds. At the atomistic level employed in molecular dynamics, such interactions demand a detailed treatment. However, to obtain mesoscopic and macroscopic level descriptions using DPD, the microscopic model can be drastically simplified.

In order to model immiscible fluids, the simplest modification to the one-component dissipative particle dynamics algorithm is to introduce a new variable, called the "color" by analogy with Rothman-Keller [20,36]. For example, we could choose red to represent oil and blue to represent water. When two particles of different color interact, we increase the conservative force, thereby increasing the repulsion. That is,

$$\alpha \mapsto \alpha_{ij} = \begin{cases} \alpha_0 & \text{if particles } i \text{ and } j \text{ are the same color} \\ \alpha_1 & \text{if particles } i \text{ and } j \text{ are different colors,} \end{cases}$$

$$(9)$$

where α_0 and α_1 are constants with $0 \leq \alpha_0 < \alpha_1$. As a consequence of mass and momentum conservation, the Navier-Stokes equation is obeyed within a single-phase DPD fluid and within regions of homogeneity of each of the two binary immiscible fluid phases [36,37,43,44]. Likewise, detailed balance is also preserved, at least in the limit of continuous time [37,43,44].

The immiscible fluids described above are identical to each other. However, it is often the case that the two fluids in a mixture will differ physically. For example, oil and water typically have different viscosities. To model binary fluids with differing viscosity, we again adopt the simplest approach: labeling one of the two phases (colors) as more viscous. When two particles of the same viscous color interact,

the dissipative (viscous) force is increased; in order to keep the temperature constant, we must correspondingly decrease the random force according to Eq. (6), i.e.,

$$\gamma \mapsto \gamma_{ij} = \begin{cases} \gamma_0 & \text{if either particle } i \text{ or } j \text{ is not the viscous color} \\ \gamma_1 & \text{if both particles } i \text{ and } j \text{ are the viscous color,} \end{cases} \tag{10}$$

$$\sigma \mapsto \sigma_{ij} = \begin{cases} \sigma_0 & \text{if either particle } i \text{ or } j \text{ is not the viscous color} \\ \sigma_1 & \text{if both particles } i \text{ and } j \text{ are the viscous color,} \end{cases} \tag{11}$$

where

$$\frac{\sigma_0^2}{\gamma_0} = \frac{\sigma_1^2}{\gamma_1} = 2k_B T. \tag{12}$$

Our previous study of finite difference methods applicable to simulations with non-conservative forces [4] indicated that the finite-difference algorithm suggested by Groot and Warren [40] is a good choice for DPD. Their method is a variation on the familiar velocity-Verlet algorithm, adding a momentum estimate before the force evaluation:

$$\mathbf{x}_i(t+\Delta t) = \mathbf{x}_i(t) + \frac{\Delta t}{m_i}\left[\mathbf{p}_i(t) + \frac{\Delta t}{2}\mathbf{f}_i(t)\right],$$

$$\mathbf{p}_i(t+\Delta t) = \mathbf{p}_i(t) + \frac{\Delta t}{2}\mathbf{f}_i(t),$$

$$\mathbf{f}_i(t+\Delta t) = \sum_{j \neq i} \mathbf{F}_{ij}(t+\Delta t), \tag{13}$$

$$\mathbf{p}_i(t+\Delta t) = \mathbf{p}_i(t) + \frac{\Delta t}{2}[\mathbf{f}_i(t) + \mathbf{f}_i(t+\Delta t)],$$

where Δt is the time step size and $\mathbf{f}_i(t)$ is the force acting on particle i at time t. The DPD units of length, mass, and time are specific to the particular set of model parameters, and the exact relationship between these parameters and a real fluid in a particular situation can be determined by considering the dimensionless groups relevant to the motion of that system, such as the Mach, Reynolds, and Weber numbers.

Many further modifications to the model have been suggested and implemented by others. Some of the most interesting include energy conservation, colloidal particles, and polymers. In very recent work, it has been shown that it is possible to derive a modified version of DPD directly from the underlying molecular dynamics [45,46].

III. TEMPORAL BEHAVIOR OF THE CHARACTERISTIC DOMAIN SIZE

A central quantity in the study of growth kinetics is the characteristic domain size $R(t)$. For binary systems in the regime of sharp domain walls, this is usually thought to follow algebraic growth laws of the form

$$R(t) \sim t^\beta. \tag{14}$$

For symmetric quenches without hydrodynamic interactions, dynamical scaling theory and experiment [47] indicate that the scaling exponent $\beta = \frac{1}{3}$. If flow effects are relevant, typically

$$\beta = \begin{cases} \frac{1}{2} & \text{for } R \ll R_h \quad \text{(diffusive)} \\ \frac{2}{3} & \text{for } R \gg R_h \quad \text{(inertial hydrodynamic)} \end{cases} \tag{15}$$

in two dimensions, and

$$\beta = \begin{cases} \frac{1}{3} & \text{for } R \ll R_d \qquad \text{(diffusive)} \\ 1 & \text{for } R_d \ll R \ll R_h \quad \text{(viscous hydrodynamic)} \\ \frac{2}{3} & \text{for } R \gg R_h \qquad \text{(inertial hydrodynamic)} \end{cases} \tag{16}$$

in three dimensions, where $R_h = \eta^2/(\rho\kappa)$ is the hydrodynamic length and $R_d = \sqrt{\eta D}$ is the diffusive length, expressed in terms of the absolute (dynamic) viscosity η, density ρ, surface tension coefficient κ, and diffusion coefficient D. These scaling laws follow directly from dimensional analysis of the macroscopic fluid dynamics equations (so-called model H, or Cahn-Hilliard coupled to Navier-Stokes hydrodynamics) in the appropriate regimes [47]. When $R \ll R_d$ in three dimensions, diffusive effects dominate and we expect the domains to form via the Lifshitz-Slyozov-Wagner (LSW) evaporation-condensation mechanism [47]. When $R \gg R_h$ in both two and three dimensions, we expect the growth mechanism to be surface tension driven by hydrodynamic flow, balanced by inertial effects [48]. If $R_d \ll R \ll R_h$ in three dimensions, we expect viscous hydrodynamic effects to dominate, as predicted by Siggia [49]; in this regime, the surface tension drives the transport of the fluid along the interface, which is possible only if both phases are continuous [47,49]. This third growth regime cannot occur in two dimensions, and so we expect to see diffusive growth for $R \ll R_h$ [48]. Due to our choice of model parameters and the small size of our simulations, we do not expect to probe the viscous or inertial hydrodynamic regimes.

Simulations in two spatial dimensions are especially useful to emphasize the importance of correct hydrodynamics: simulations which do not conserve momentum typically give $\beta = \frac{1}{3}$ for the diffusive regime ($R \ll R_h$) [1–3,24–26]. Simulation methods with correct hydrodynamic interactions typically give the expected result of $\beta = \frac{1}{2}$ (see, e.g., Refs. [1–3,6,7,10,16]). It is worth noting that momentum conservation is not thought necessary to model spinodal decomposition in binary metallic alloys, since phase separation occurs

by the migration of atoms to neighboring vacancies on the crystalline lattice [50]. Simulations based on lattice-Boltzmann techniques also typically display $\beta = \frac{1}{3}$. These observations are supported by a renormalization-group approach which has shown that thermal fluctuations cause Brownian motion-driven coalescence and play a crucial role in causing β to assume the value of $\frac{1}{2}$ [47]; although some lattice-Boltzmann techniques include these fluctuations [29], most do not.

There is some confusion in the literature over which scaling exponents should be observed for off-critical quenches, and whether or not the algebraic scaling law [Eq. (14)] should in fact be obeyed for any off-critical binary immiscible fluid. Several authors have reported the coexistence of multiple length scales [27,34,51]. It is likewise uncertain as to what behavior should be observed from binary immiscible fluids of differing viscosity [35]. Certainly, one growth mechanism we expect for off-critical quenches of both equal and differing viscosity is the LSW evaporation-condensation mechanism, for which $\beta = \frac{1}{3}$ [47].

It should also be noted that there are still some experimental and theoretical challenges in unraveling the behavior of systems in which both the order parameter and the momentum are locally conserved [47]. Experimentally, for example, it is difficult if not impossible to study two-dimensional fluid systems. As far as numerical studies are concerned, it is important to recognize that three-dimensional simulations are particularly demanding on all the aforementioned techniques, and so definitive results are harder to come by than in two dimensions.

Indeed, Cates's group in Edinburgh has recently reported somewhat conflicting results from three-dimensional studies of binary immiscible fluid separation for equal viscosity fluids using dissipative particle dynamics and lattice-Boltzmann methods [5,52]. While the former suggests the persistence of nonuniversal length scales, hypothesized to be due to the intrusion of a ''molecular'' or discretization length scale, this is not supported by the latter, from which finite-size effects were more rigorously excluded. Note, however, that whereas the lattice-Boltzmann scheme was based on a Landau free-energy approach, and is essentially no more than a finite-difference solution of the continuum model H equations, the macroscopic equations to which the spinodal DPD scheme corresponds have not yet been derived. This makes it unclear whether the two systems being simulated are really one and the same. Both of these studies emphasize the importance of observing dynamical scaling over decades of time before drawing conclusions as to the true nature of the scaling regime. One notable result of their work is the clarification of the relative time scales over which computer simulation techniques typically operate. For the simulations they discuss, molecular-dynamics time scales are on the order of 10^2 in dimensionless units, lattice-gas automata and Langevin dynamics probe time scales on the order of 10^2 through 10^4, DPD typically 10^3 to 10^5, and methods based on the lattice-Boltzmann equation 10^1 through 10^8.

Grant and Elder have recently argued [53] that $\beta \leq \frac{1}{2}$ in any asymptotic scaling regime because the Reynolds number $\mathrm{Re} = \rho R V / \eta$ (where V is a characteristic velocity) cannot diverge, and in fact must remain less than a critical value $\mathrm{Re}_{\mathrm{cr}}$ to avoid the onset of turbulence [54] and possible tur-

bulent remixing of the fluids. The conclusion they draw is that the $\beta = \frac{2}{3}$ scaling regime must be transient [53]. However, their analysis neglects mention of the relative strength of the interface, quantified, for example, by the Weber number $N_{\mathrm{We}} = \rho R V^2 / \kappa$. If N_{We} is small at the onset of turbulence, we would expect turbulent remixing to be delayed, or perhaps even postponed indefinitely allowing Re to diverge. In any case, the separation dynamics would likely be affected by $\mathrm{Re} \gtrsim \mathrm{Re}_{\mathrm{cr}}$; for example, the fluid viscosity in a turbulent region is roughly proportional to Re [54].

IV. ESTIMATING THE CHARACTERISTIC DOMAIN SIZE

In order to characterize the phase separation kinetics within a binary immiscible fluid, we need a practical tool to measure the characteristic domain size corresponding to the state of the system at a given point in time. The use of the static structure function for this purpose is widespread. However, we have noticed bizarre ''early time'' behavior when using the static structure function to characterize simulations of highly off-critical quenches. Specifically, the characteristic domain size would sometimes change suddenly by an order of magnitude. This abrupt change in behavior did not correspond to anything observable in the time evolution of the positions of the DPD particles. Such anomalous behavior is likely due to the large fluctuations prevalent in the static structure function for small simulations of highly mixed binary fluids, for which the characteristic domain size is very small.

The radial distribution function $g(r)$ is a well-established tool for the analysis of single-phase fluids [55,56], and indicates the likelihood of finding two particles separated by a distance r. For binary fluids we can also use the same-phase and differing-phase distribution functions [6]. The same-phase distribution function $g_{00}(r)$ describes the likelihood of finding two particles of the *same* phase separated by a distance r, and the differing-phase distribution function $g_{01}(r)$ describes the likelihood of finding two particles of *differing* phase separated by a distance r. From the peaks of the differing-phase radial distribution function, we can estimate the characteristic separation of particles of differing phase (i.e., the characteristic domain size). Consequently, we decided to calculate the distribution between particles of different phase (color),

$$g_{01}(r) = \frac{m \, n(r, \Delta r)}{\rho N \phi [1 - \phi] V(r, \Delta r)}, \quad (17)$$

where $m = m_i \; \forall i$ is the mass of each particle (assumed all identical), $n(r, \Delta r)$ is the number of particle pairs of differing phase with separation between $r - \Delta r/2$ and $r + \Delta r/2$, N is the total number of particles, $\phi \in (0,1)$ is the fraction of particles of one phase (the more viscous phase if the two phases are of different viscosity), and $V(r, \Delta r)$ is the volume of the spherical shell of radius r and thickness Δr (from $r - \Delta r/2$ to $r + \Delta r/2$). It is apparent from Eq. (17) that $g_{01}(r)$ can only be calculated for $r \leq L/2$ in a simulation with a periodic box size of L; this should not be interpreted as an undesirable limitation as finite-size effects are normally significant for $R > L/2$ [5,52]. A value of $\Delta r = L/2000$ gives a

reasonable compromise between noise and resolution for the size of simulation we discuss in this paper.

The principal difficulty lies in analyzing the results automatically, as we need to calculate $g_{01}(r)$ at many time steps within each simulation in order to display the domain growth over time. We chose to calculate the median of that portion of the smoothed $g_{01}(r)$ curve extending above a threshold value $1+3s$, where s is the standard deviation of the smoothed curve when it has effectively a constant unit value, estimated from the last tenth of the smoothed $g_{01}(r)$ curve at $t=1$. We used a fourth-order Savitzky-Golay smoothing filter [57,58] to smooth $g_{01}(r)$ over r at each point in time with a symmetric window size chosen to reduce the noise while leaving significant features untouched (41 points in two dimensions and 101 points in three). We chose the cutoff threshold of $1+3s$ so as not to bias the median by the size of the periodic simulation box; likewise, we chose the median in preference to the mean (first moment) because the median is less biased by outliers, such as those 2.5% of noisy points which effectively have unit value but extend above the threshold. Both the median and mean give poor estimates of the characteristic domain size as it approaches $L/2$, the limit of calculable $g_{01}(r)$. When this situation is detected, we use the global maximum of $g_{01}(r)$ to estimate the domain size instead; this is a continuous transition for symmetrical peaks.

Once we have calculated the characteristic domain size for a series of $g_{01}(r)$ curves taken at different times from a single simulation, we begin a search for linear sections in the plot of $\log_{10} R$ versus $\log_{10} t$. This has also been automated, using analysis of variance to decide whether a given section of the plot is linear or cubic. We used the analytic expressions for the least-squares fits with moments taken about the means to minimize the effect of roundoff error. We keep only the longest linear sections, subject to there not being any significant gaps in the coverage of the log-log plot. An ensemble average of a number of simulations yields a plot of the scaling exponent β versus $\log_{10} t$, in which long horizontal (zero gradient) sections represent algebraic growth. This procedure allows more accurate determination of the scaling exponent than a visual comparison of $\log_{10} R$ versus $\log_{10} t$ to a straight line of a particular slope, and provides a statistically valid determination of whether or not the growth is truly algebraic over a particular time period. Finite-size effects for $R \approx L/2$ normally result in nonalgebraic growth or unusually low scaling exponents; either case is easily detected by our method. A further advantage is the automation we have described, permitting large ensemble averages with minimal effort.

We should note that estimating the characteristic domain size using the median can occasionally lead to discontinuities. If these discontinuities are large enough, they will cause a break between linear sections. Small discontinuities may be spanned by a single line, which would affect the slope (β) and be detrimental to the results. However, large discontinuities will not be spanned, and so will not affect the slope.

The results we obtained using these techniques are considerably better than those obtained with the static structure function, especially for highly mixed fluids where the pair distribution function is not drowned by fluctuations to the extent that the static structure function is. Furthermore, the

TABLE I. Model parameters for the viscosity measurements of the lower-viscosity fluid.

Model parameter	Value
α	7.063
γ	5.650
σ	1.290
m_i	1
r_c	1.3
ρ	4

pair distribution function is more intuitive to analyze than the static structure function, which aids our interpretation of the results.

V. SIMULATION RESULTS

For the simulations of fluids with differing viscosity, we chose one phase to be an order of magnitude more viscous than the other, i.e., $\gamma_1 = 10\gamma_0$. Before simulating this new complex fluid, it is advisable to verify that increasing the parameter γ, while keeping the temperature constant, does indeed increase the viscosity. For the lower-viscosity fluid we chose the model parameters shown in Table I. The absolute (dynamic) viscosity of a homogeneous DPD fluid can be estimated theoretically from the continuous-time viscosity, ignoring the effect of the conservative forces (i.e., $\alpha = 0$) [59,60]; the continuous-time viscosity of this lower-viscosity fluid is $\eta = 2.8$.

In order to verify this estimate, we performed a series of simulations of steady shear using Lees-Edwards periodic boundary conditions. We performed a total of 63 simulations with a time step of $\Delta t = 0.1$ (in our DPD time units), each from a different random initial configuration and each allowed to settle to steady-state shear before measurement began. We studied systems of both 1600 and 6400 particles, six simulations at each of nine different shear rates for the former and three simulations at each of three distinct shear rates for the latter. As the results from the larger simulations gave a mean viscosity nearly identical to that of the smaller ones, we can conclude that finite-size effects do not bias the viscosity of the smaller, faster simulations. We calculated the velocity profile for each set of parameters, and found it to be statistically indistinguishable from linear in every case.

Analyzing these simulations led to a conclusion of $\eta = 1.94 \pm 0.01$. Others have also found discrepancies between theory and simulation, particularly regarding the kinematic contribution to viscosity [59], so the difference between the simulated viscosity and the continuous-time viscosity is not entirely surprising. Since molecular-dynamics simulations containing only conservative forces give a finite viscosity, we would be surprised if the theoretical estimate did not differ from our calculations.

In order to measure the viscosity of the more viscous fluid, we set up a series of 1600 particle simulations of a homogeneous DPD fluid as described above, using a total of 30 simulations. We varied the shear rate in the range that gave the best results in the previous simulations. The model parameters differed in that γ was a factor of 10 larger while

TABLE II. Model parameters for the viscosity measurements of the higher-viscosity fluid.

Model parameter	Value
α	7.063
γ	56.50
σ	4.079
m_i	1
r_c	1.3
ρ	4

σ was a factor of $\sqrt{10}$ larger to keep the temperature constant [see Eq. (12)]; these parameters are shown in Table II. We decreased the time step to $\Delta t = 0.01$ due to the increased magnitude of the dissipative and stochastic forces. Analyzing these results led to the conclusion that $\eta = 17.2 \pm 0.3$, which confirms the increase in viscosity. This increase is close to a factor of 10, so that for similar model parameters it is reasonable to conclude that γ is approximately proportional to viscosity.

It is possible to measure the surface tension of a binary immiscible fluid by integrating the pressure tensor across a flat interface, or by verifying Laplace's law for a series of equilibrium bubbles of varying radii [55]. Laplace's law was verified for a DPD binary immiscible fluid in our previous simulations [1–3], and so surface tension measurements were omitted from the present study. These calculations would, however, allow identification of the unit of time for comparison with other simulation techniques (see, e.g., Refs. [5,52]). Theoretical estimates for surface tension are also available, but are of similar accuracy to the viscosity estimate above.

For the simulation of fluids of differing viscosity, we must also choose the relatively small time step size of $\Delta t = 0.01$ in order to ensure the stability of the algorithm as a result of the increased magnitude of the dissipative forces. This has the consequence of making these simulations computationally much more expensive than equal-viscosity simulations. In this context, it is worth commenting on the virtues of using DPD to perform simulations of differing-viscosity fluids compared with other models. Sappelt and Jäckle use an approach based on the Cahn-Hilliard equation (so-called model

TABLE III. Model parameters used for the differing-viscosity immiscible fluid simulations.

Model parameter	Value
α_0	7.063
α_1	7.487
γ_0	5.650
γ_1	56.50
σ_0	1.290
σ_1	4.079
m_i	1
r_c	1.3
ρ	4

TABLE IV. Scaling exponents for two-dimensional differing-viscosity fluids as a function of viscous phase fraction, divided into ''early'' and ''late time.''

ϕ	Approximate range of $\log_{10} t$	β
0.2	0.17 ± 0.09 to 1.28 ± 0.09	0.092 ± 0.014
0.3	0.09 ± 0.04 to 1.07 ± 0.03	0.083 ± 0.008
0.4	0.13 ± 0.05 to 1.13 ± 0.04	0.068 ± 0.006
0.5	0.13 ± 0.05 to 1.05 ± 0.06	0.058 ± 0.009
0.6	0.15 ± 0.05 to 1.01 ± 0.09	0.042 ± 0.010
0.7	0.24 ± 0.05 to 1.25 ± 0.07	0.058 ± 0.010
0.8	0.16 ± 0.13 to 1.25 ± 0.11	0.031 ± 0.014
0.9	0.02 ± 0.05 to 1.11 ± 0.12	-0.24 ± 0.07
0.1	0.26 ± 0.19 to 2.57 ± 0.11	0.291 ± 0.016
0.2	0.53 ± 0.13 to 2.63 ± 0.08	0.335 ± 0.008
0.3	0.72 ± 0.05 to 2.51 ± 0.07	0.333 ± 0.012
0.4	0.72 ± 0.06 to 2.45 ± 0.08	0.341 ± 0.016
0.5	0.83 ± 0.09 to 2.47 ± 0.06	0.336 ± 0.016
0.6	0.92 ± 0.11 to 2.52 ± 0.07	0.336 ± 0.012
0.7	0.95 ± 0.04 to 2.65 ± 0.06	0.316 ± 0.010
0.8	1.03 ± 0.10 to 2.66 ± 0.07	0.299 ± 0.013
0.9	0.55 ± 0.08 to 2.56 ± 0.13	0.20 ± 0.02

B without noise) with a concentration-dependent mobility [35], so they do not include hydrodynamics, unlike our approach with DPD. The other mesoscale techniques which could be used to model these fluids include lattice-gas automata and methods based on the lattice-Boltzmann equation. As with DPD, there is a high computational price to the lattice-gas approach, which requires adjustment to the collisional outcomes of the look-up tables. Lattice-Boltzmann

TABLE V. Scaling exponents for three-dimensional differing-viscosity fluids as a function of viscous phase fraction, divided into ''early'' and ''late time.''

| ϕ	Approximate range of $\log_{10} t$	β
0.1	0.02 ± 0.05 to 1.74 ± 0.05	0.023 ± 0.002
0.2	-0.012 ± 0.015 to 1.12 ± 0.04	0.0219 ± 0.0014
0.3	0 to 0.92 ± 0.03	0.0171 ± 0.0017
0.4	0.02 ± 0.04 to 0.88 ± 0.05	0.025 ± 0.005
0.5	0.00 ± 0.02 to 0.87 ± 0.04	0.028 ± 0.007
0.6	-0.008 ± 0.016 to 1.00 ± 0.02	0.0273 ± 0.0012
0.7	0.06 ± 0.05 to 1.03 ± 0.04	0.022 ± 0.003
0.8	-0.004 ± 0.012 to 1.31 ± 0.04	0.0228 ± 0.0013
0.9	0.06 ± 0.08 to 1.95 ± 0.09	0.021 ± 0.003
0.1	1.47 ± 0.07 to 2.62 ± 0.07	0.53 ± 0.05
0.2	0.78 ± 0.04 to 2.67 ± 0.05	0.377 ± 0.008
0.3	0.79 ± 0.13 to 2.67 ± 0.08	0.376 ± 0.010
0.4	0.71 ± 0.16 to 2.68 ± 0.06	0.360 ± 0.007
0.5	0.65 ± 0.05 to 2.68 ± 0.05	0.358 ± 0.007
0.6	0.703 ± 0.019 to 2.64 ± 0.08	0.364 ± 0.007
0.7	0.85 ± 0.06 to 2.62 ± 0.10	0.363 ± 0.012
0.8	1.08 ± 0.04 to 2.51 ± 0.06	0.406 ± 0.017
0.9	1.76 ± 0.08 to 2.70 ± 0.03	0.52 ± 0.02
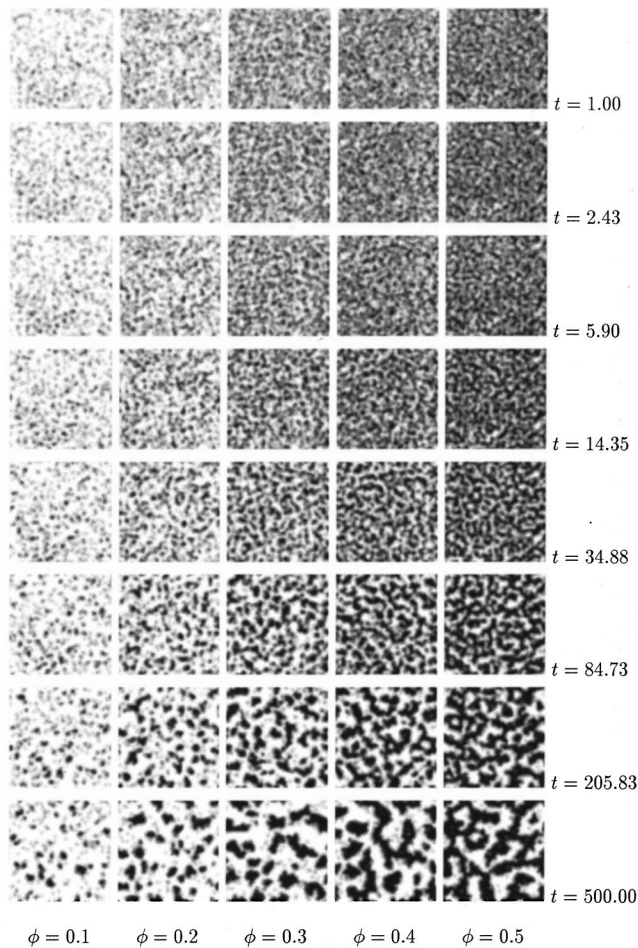
FIG. 1. Time evolution of five sample simulations of two-dimensional differing-viscosity fluids, each simulation having a different viscous phase fraction (varying from $\phi = 0.1$ through $\phi = 0.5$).
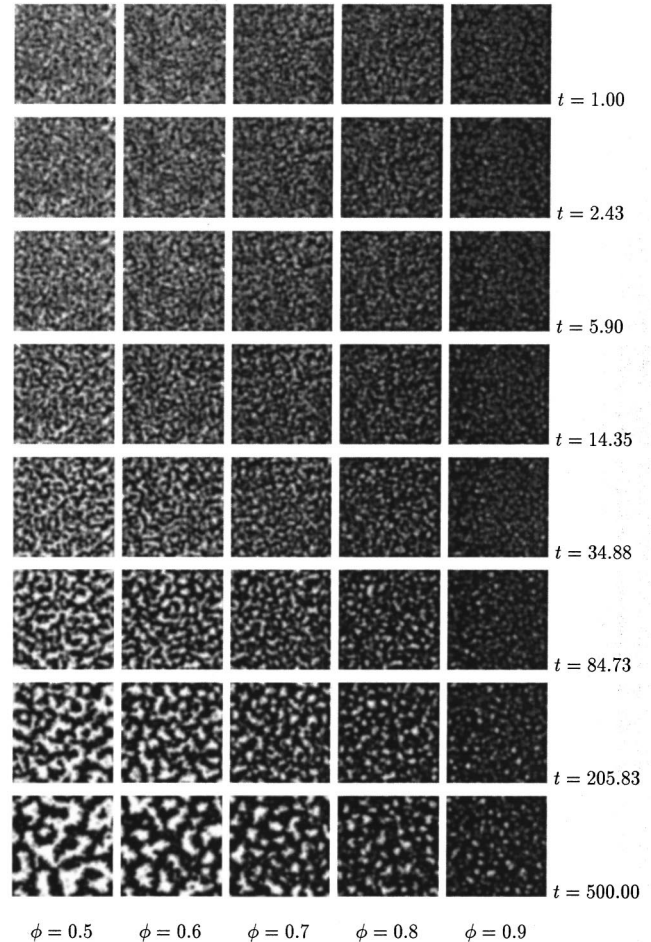

FIG. 2. Time evolution of five sample simulations of two-dimensional differing-viscosity fluids, each simulation having a different viscous phase fraction (varying from $\phi = 0.5$ through $\phi = 0.9$).

(more correctly, lattice-BGK) models can be used, based, for example, on the Swift-Osborn-Yeomans free-energy functional approach [61], but there is a similar computational price, although with the additional complication of poorly understood numerical instabilities. However, DPD offers the simplest algorithmic implementation which is thermodynamically consistent.

Our differing-viscosity simulations used the model parameters shown in Table III. Each simulation had 6400 particles, and ran for 50 000 time steps. We chose to use only 6400 particles in our simulations so that individual simulations would be quick enough to be run multiple times, allowing us to consider the effect of changing the phase fraction and viscosity, and to increase the confidence in our results and calculate accurate error estimates with ensemble averaging. Simulations with more particles would have given better resolution of small scale features (relative to the system size) and postponed the finite-size effects, at the price of increased computational demands. Our resources would only have allowed a few simulations of the size and length used by Jury *et al.* [5] (1 000 000 particles), making studies of the sort we describe in this paper impossible.

We calculated the pair distribution function at 64 logarithmically spaced points in time during the course of each

simulation, starting from time $t = 1$ and finishing at $t = 500$ (in our DPD time units). In both two and three dimensions, we performed ten simulations at each of nine different fractions of the viscous phase, ranging from $\phi = 0.1$ (10% viscous phase) to $\phi = 0.9$ (90% viscous phase). We show the time evolution of a single simulation at each value of the viscous fraction in Figs. 1–4 for both two and three dimensions. We represent the positions of the DPD particles in two dimensions by a gray scale map, in which the particle positions are weighted by Eq. (7) and assigned an intensity of gray based upon the proportion of each phase in this localized average. Figures 3 and 4 display the three-dimensional surface of the interface between the two immiscible phases, as defined by there being equal proportions of each fluid in the localized average. In these four figures the gradual development of domains can be seen. We examined the results of the domain size analysis for each simulation in plots of $\log_{10} R$ versus $\log_{10} t$, and further examined each ensemble average in plots of β versus $\log_{10} t$; the latter yielded the mean values of β and corresponding 68% confidence intervals for significant sections of algebraic growth. We show these results for two and three dimensions in Tables IV and V and Figs. 5 and 6. The range of $\log_{10} t$ we give in the tables should be taken as a rough guide, since there is often
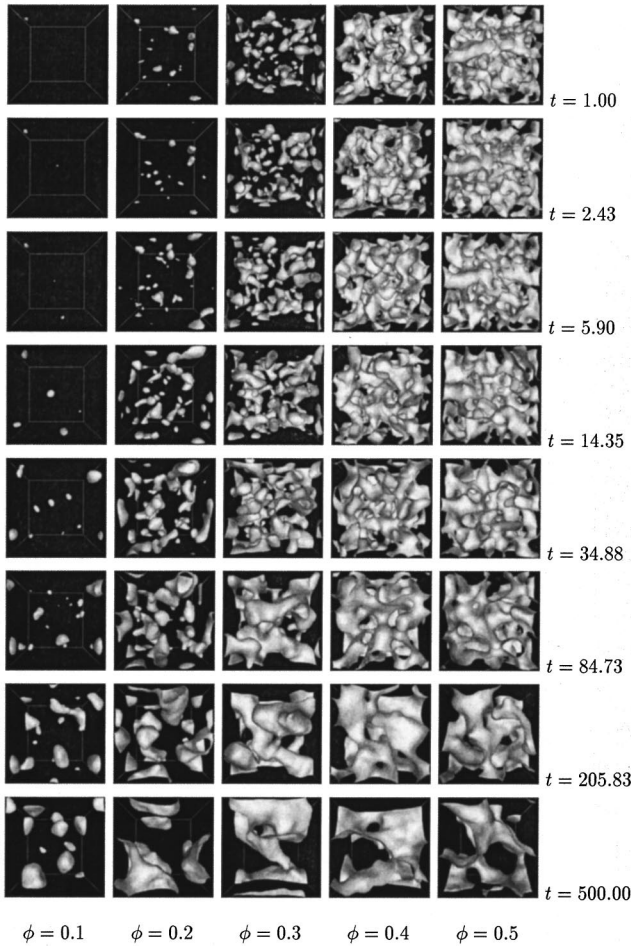
FIG. 3. Time evolution of five sample simulations of three-dimensional differing-viscosity fluids, each simulation having a different viscous phase fraction (varying from $\phi = 0.1$ through $\phi = 0.5$).
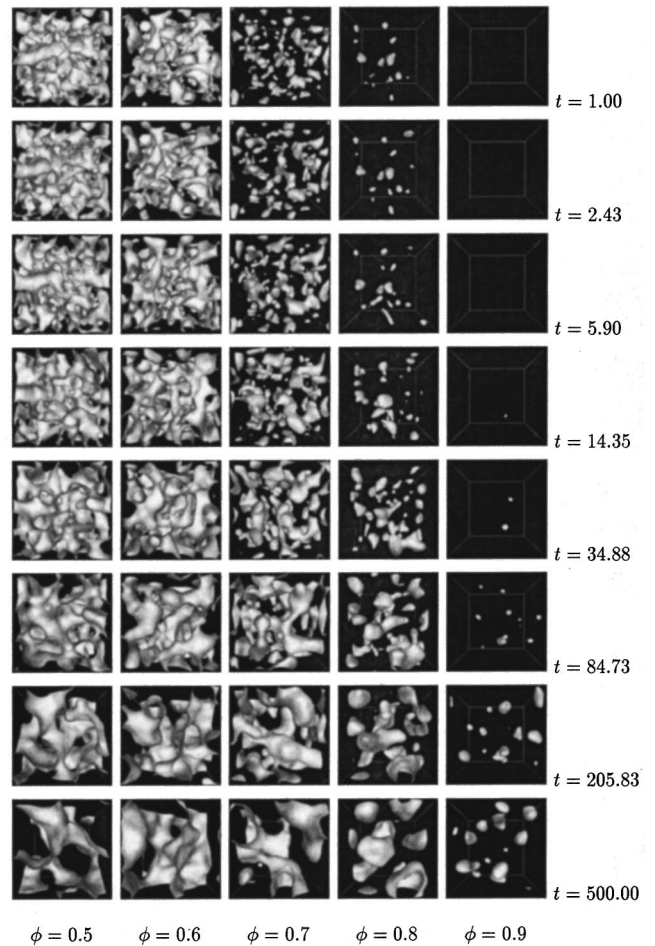

FIG. 4. Time evolution of five sample simulations of three-dimensional differing-viscosity fluids, each simulation having a different viscous phase fraction (varying from $\phi = 0.5$ through $\phi = 0.9$).

a high degree of correlation between the start and end times of a particular linear section and its growth exponent within the broad category of late time. We should emphasize that we are using the term ''late time'' as a relative category in this paper, to distinguish these results from those obtained at very early times. Due to the model parameters and small size of these simulations, we do not expect to probe the viscous or inertial hydrodynamic regimes [see Eqs. (14)–(16), and compare with Refs. [1–4]].

We also constructed a series of equal-viscosity simulations in both two and three dimensions. These had $\Delta t = 0.1$, 6400 particles, and stopped at $t = 1000$. The model parameters were the same as in the differing-viscosity simulations, with the exception that both phases were identical to the less-viscous phase of the differing-viscosity simulations (i.e., $\gamma = \gamma_0$ and $\sigma = \sigma_0$). We calculated the pair distribution function at 64 different points from $t = 1$ to $t = 1000$, with ten simulations at each of eight different minority phase fractions from $\phi = 0.05$ to $\phi = 0.5$ in two dimensions, and ten simulations at each of five different fractions from $\phi = 0.1$ to $\phi = 0.5$ in three dimensions. We show the time evolution of a single simulation at each value of the minority fraction in Figs. 7 and 8 for two and three dimensions, respectively. In these two figures the gradual development of domains can be

seen, and is greatly slowed for small minority fraction. We show the scaling exponents for two- and three-dimensional equal-viscosity fluids in Tables VI and VII and Figs. 9 and 10, where we mirror the scaling exponents about $\phi = 0.5$ to show the full range of minority phase fraction. Comparison with Figs. 7 and 8 qualitatively confirms the same behavior.

VI. DISCUSSION

A feature common to all these simulations is the lack of scale invariance at very early times, until approximately $t = 10$ to $t = 50$ (in our DPD time units) depending on the exact composition of the fluid. This is apparent in the $g_{01}(r)$ curves as multiple peaks of similar magnitude, but could not be seen in the frequency domain shown by the static structure function. Figure 11 shows an example of the differing-phase radial distribution function for a three-dimensional equal-viscosity simulation ($\phi = 0.5$) at $t = 13.9$; the crosses represent the actual data and the curve represents the smoothed data. This is one of the simulations we show in Fig. 8. The multiple peaks typically evolve by changing their height and relative weight, but not their position. This is noticeably different from our ''late time'' behavior of the distribution function, where a single peak gradually advances
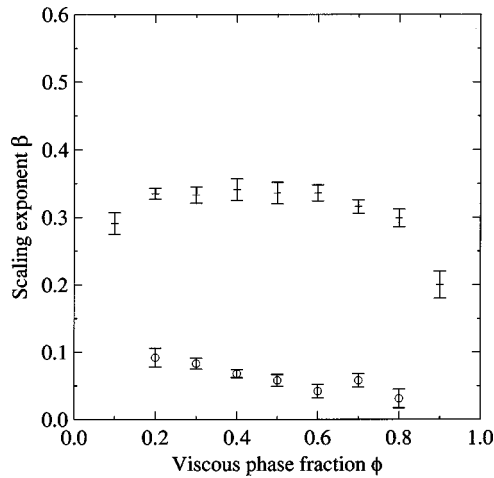
FIG. 5. Scaling exponents for two-dimensional differing-viscosity fluids as a function of viscous phase fraction. Circles indicate ''early time'' and horizontal marks ''late time''; error bars are 68% confidence intervals.

its position while broadening but retaining its height and general shape. It is because of this ''early time'' behavior that it was decided not to use solely the global maximum of $g_{01}(r)$ to estimate the characteristic domain size.

At these ''early times'' in all of the simulations, we observed algebraic growth with a very small exponent, roughly 0.126 ± 0.003 in two-dimensional equal-viscosity simulations, 0.062 ± 0.009 in two-dimensional differing-viscosity simulations [except $\phi=0.9$ (90% viscous phase), for which $\beta=-0.24\pm0.07$], and 0.0246 ± 0.0008 for simulations in three dimensions. This corresponds to the region of breakdown of scale invariance we described at the beginning of this section. These ''early time'' exponents are unaffected by viscous or minority phase fraction in all of the simulations, except the differing-viscosity simulations in two dimensions. Here β decreases with increasing ϕ (viscous phase fraction), probably due to the domain-growth arresting effect of increasing viscosity. We observed a remarkable (though short) regime of $\beta=-0.24\pm0.07$ for $\phi=0.9$ (90% viscous phase),
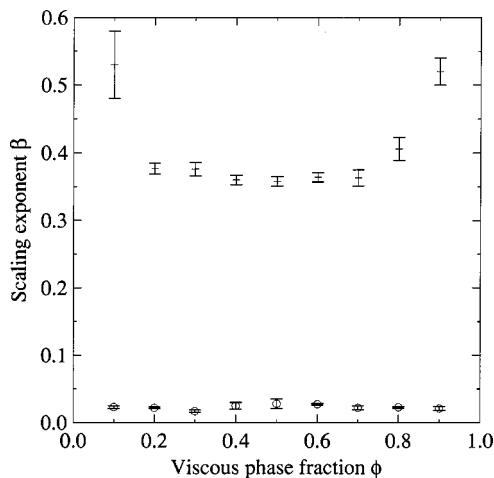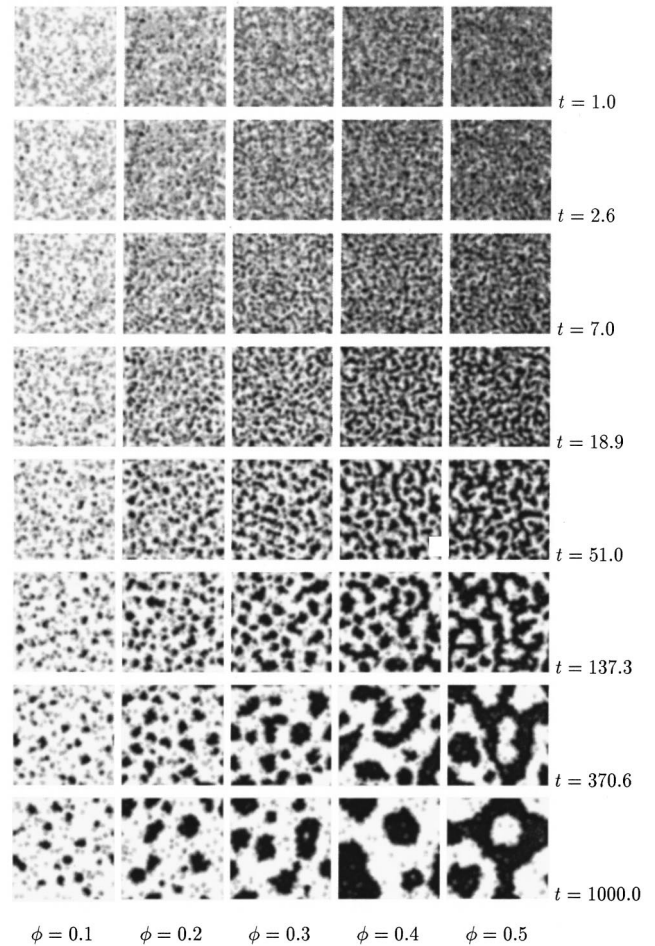

FIG. 7. Time evolution of five sample simulations of two-dimensional equal-viscosity fluids, each simulation having a different minority phase fraction (varying from $\phi=0.1$ through $\phi=0.5$).

for which we have no adequate explanation. Others normally discard similar early time regimes without comment [9,16,29,30,32,33,35] or as an ''early stage'' or ''transient'' regime [5,29]. However, there is growing evidence for the coexistence of multiple domain sizes and hence a breakdown in universality, at least in certain phase-ordering domains [27,34,51].

For ''late time'' domain growth in the two-dimensional differing-viscosity simulations (see Fig. 5), we observed a fairly constant value of β for $\phi=0.2$ (20% viscous phase) through $\phi=0.6$ (60% viscous phase), decreasing both for $\phi=0.1$ and very slightly for $\phi=0.7$ and $\phi=0.8$, then decreasing sharply at $\phi=0.9$. This asymmetry is consistent with the variation of the ''early time'' exponent in that an increasingly viscous fluid is expected to develop domains more gradually. At increasingly rarefied fractions ($\phi=0.1$ and $\phi=0.9$), domain growth is retarded by the increased isolation of the droplets. The ''late time'' growth exponent throughout is effectively $\frac{1}{3}$, which suggests that the presence of fluids of differing viscosity interferes with the normal $\beta=\frac{1}{2}$ growth mechanism in two dimensions. The growth exponent of $\frac{1}{3}$ is expected from the LSW evaporation-condensation mechanism [47]. This is in some ways analogous to the effect obtained by deliberately breaking

FIG. 6. Scaling exponents for three-dimensional differing-viscosity fluids as a function of viscous phase fraction. Circles indicate ''early time'' and horizontal marks ''late time''; error bars are 68% confidence intervals.
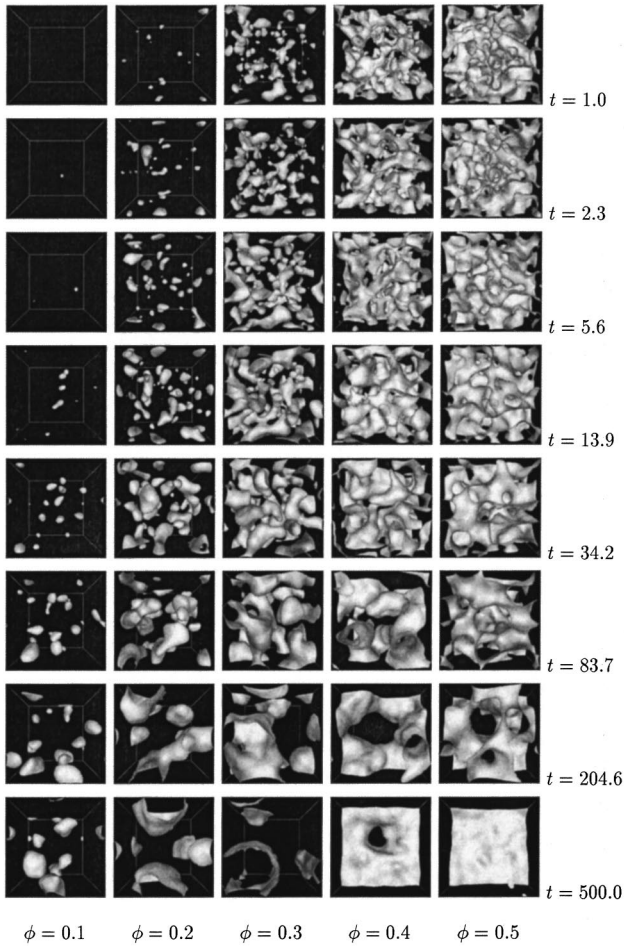
FIG. 8. Time evolution of five sample simulations of three-dimensional equal-viscosity fluids, each simulation having a different minority phase fraction (varying from $\phi = 0.1$ through $\phi = 0.5$).

TABLE VI. Scaling exponents for two-dimensional equal-viscosity fluids as a function of minority phase fraction, divided into ''early'' and ''late time.''

ϕ	Approximate range of $\log_{10} t$	β
0.2	0 to 1.10 ± 0.04	0.123 ± 0.016
0.25	0.02 ± 0.04 to 1.04 ± 0.06	0.13 ± 0.02
0.3	0.02 ± 0.08 to 1.00 ± 0.05	0.135 ± 0.012
0.4	-0.015 ± 0.010 to 0.85 ± 0.03	0.114 ± 0.017
0.5	0.00 ± 0.03 to 0.90 ± 0.08	0.13 ± 0.03
0.05	0.19 ± 0.19 to 2.83 ± 0.14	0.283 ± 0.019
0.1	0.12 ± 0.16 to 2.81 ± 0.18	0.304 ± 0.010
0.15	0.24 ± 0.20 to 2.71 ± 0.18	0.304 ± 0.010
0.2	0.52 ± 0.24 to 2.71 ± 0.15	0.337 ± 0.012
0.25	1.0 ± 0.3 to 2.76 ± 0.13	0.39 ± 0.04
0.3	0.71 ± 0.15 to 2.53 ± 0.22	0.367 ± 0.016
0.4	1.11 ± 0.16 to 2.5 ± 0.2	0.415 ± 0.019
0.5	1.4 ± 0.3 to 2.50 ± 0.09	0.47 ± 0.04

would be the $\beta = \frac{1}{3}$ LSW evaporation-condensation mechanism [47]; it may be a combination of these two mechanisms that leads to our observed $\frac{1}{3} < \beta < \frac{2}{3}$ growth. A slight asymmetry in the ''late time'' growth exponent is also evident, with domain growth proceeding more slowly with increasingly viscous fluids of non-extreme viscous fraction.

For equal-viscosity fluids in two dimensions we observed the expected $\beta = \frac{1}{2}$ for symmetric quenches ($\phi = 0.5$) [1–3]. As we reduced the minority phase fraction, we observed a steady decrease in the scaling exponent until $\beta = \frac{1}{3}$ is reached at the extremes. This confirms the results of other workers [27] that increasingly off-critical quenches retard the domain growth, while providing support for the observed slowdown of growth at the extremes of viscous fraction in differing-viscosity fluids in two dimensions, which we commented on above.

In three dimensions, the domain growth of equal-viscosity fluids appears largely unaffected by varying the minority phase fraction. Although there may be some increase in β at the extremes of ϕ (as seen in the differing-viscosity fluid in three dimensions), this is difficult to confirm definitely because of the large variation in the rate of growth observed for the simulations with $\phi = 0.1$, and hence the correspondingly large confidence interval. The scaling exponent throughout is close to $\beta = \frac{1}{3}$. Whereas Jury et al. [5] were intending to probe the viscous or inertial hydrodynamic regimes with their DPD simulations of equal-viscosity fluids in three dimensions, we aimed only to probe length scales below R_d and R_h [see Eqs. (14)–(16)]. As such, our results are fully consistent with theirs. Our exclusion of finite-size effects is more rigorous than theirs, and although not as extreme as that advocated by Kendon et al. [52], our method gives statistical confidence that these domains are scaling algebraically. Both Jury et al. [5] and Kendon et al. [52] were able to cover the time domain more fully in three-dimensional equal-viscosity symmetric quenches only at the cost of performing a large number of computationally very intensive and very expensive simulations.

momentum conservation in symmetric quenches, as described previously [1–3]. Our domains are considerably less circular at all viscous fractions than those observed by Sappelt and Jäckle (compare Figs. 1 and 2 with Ref. [35]). This is likely due to the lack of hydrodynamic interactions in their model and to the greater difference in viscosity between their two phases. As in their simulations, our two-phase structure for fluids of differing viscosity is not very different from the structure for fluids of equal viscosity. Moreover, our simulations do not reveal any new insights regarding interfacial structure.

In three dimensions, the ''late time'' domain growth of differing-viscosity fluids displays nearly the opposite behavior, with the scaling exponent increasing as the viscous fraction reaches its extremes. This could be explained by the increased fluid mobility in simulations with an extra spatial dimension, as the majority phase is completely connected and so the domain growth could occur according to the $\beta = \frac{2}{3}$ mechanism, which is surface tension driven by hydrodynamic flow, balanced by inertial effects. This is qualitatively substantiated by inspection of Figs. 3 and 4, where a larger degree of connectivity of the majority phase can be observed at the extremes of viscous fraction than for $\phi \approx 0.5$. However, a more obvious mechanism for the domain growth

TABLE VII. Scaling exponents for three-dimensional equal-viscosity fluids as a function of minority phase fraction, divided into ''early'' and ''late time.''

ϕ	Approximate range of $\log_{10}t$	β
0.1	0 to 1.41 ± 0.07	0.028 ± 0.013
0.2	0.01 ± 0.04 to 0.90 ± 0.04	0.026 ± 0.007
0.3	0.00 ± 0.04 to 0.73 ± 0.05	0.026 ± 0.007
0.4	0 to 0.61 ± 0.05	0.023 ± 0.005
0.5	0 to 0.60 ± 0.05	0.029 ± 0.006
0.1	1.35 ± 0.11 to 2.48 ± 0.18	0.43 ± 0.08
0.2	0.52 ± 0.04 to 2.68 ± 0.02	0.362 ± 0.008
0.3	0.43 ± 0.04 to 2.53 ± 0.04	0.366 ± 0.009
0.4	0.38 ± 0.02 to 2.47 ± 0.03	0.369 ± 0.006
0.5	0.32 ± 0.04 to 2.48 ± 0.02	0.364 ± 0.007

VII. CONCLUSIONS

In this paper, we have described simulations of the domain growth and phase separation of hydrodynamically correct binary immiscible fluids of differing and equal viscosity as a function of minority phase concentration in both two and three spatial dimensions. Due to our choice of model parameters and the small size of our simulations, we did not expect to probe the viscous or inertial hydrodynamic regimes. In three dimensions, we found that the characteristic domain size scales as $t^{1/3}$ for simulations of differing and equal-viscosity fluids developing from symmetric and slightly off-critical quenches. For highly off-critical quenches we observe an increase in the scaling exponent. In two dimensions, we also observe $t^{1/3}$ in simulations of differing-viscosity fluids developing from symmetric and slightly off-critical quenches, although we observe a decrease in the scaling exponent for highly off-critical quenches. In equal-viscosity fluids in two dimensions, we observe $t^{1/2}$ for symmetric quenches and a roughly linear decrease to $t^{1/3}$ for highly off-critical quenches; these results
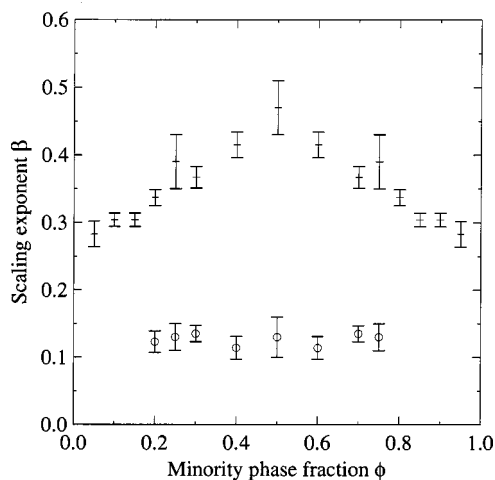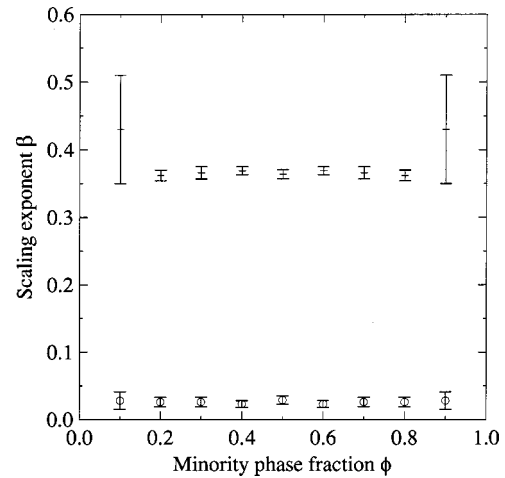

FIG. 10. Scaling exponents for three-dimensional equal-viscosity fluids as a function of minority phase fraction. Circles indicate ''early time'' and horizontal marks ''late time''; error bars are 68% confidence intervals.

are in agreement with similar lattice-gas simulations in two dimensions [27].

Obtaining meaningful results for ensemble averages of highly off-critical binary immiscible fluids was only made feasible by our automation of the calculation of the characteristic domain size by the pair correlation function. It also made possible the identification of a regime of breakdown of scale invariance at very early times, which was not noticeable in our original analysis using the static structure function. Further simulations aimed at probing the viscous and inertial hydrodynamic regimes [see Eqs. (14)–(16)] would be a useful addition to this work, as would simulations aimed at covering longer periods of time; however, both would require substantially increased computational work.

FIG. 9. Scaling exponents for two-dimensional equal-viscosity fluids as a function of minority phase fraction. Circles indicate ''early time'' and horizontal marks ''late time''; error bars are 68% confidence intervals.
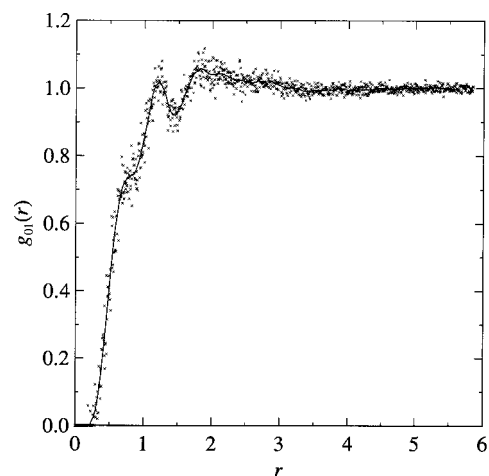

FIG. 11. Differing-phase radial distribution function for a three-dimensional equal-viscosity fluid ($\phi=0.5$) at $t=13.9$. The unit of length for r is specific to the particular set of model parameters used.

mon Jury, Colin Marsh, John Melrose, and Julia Yeomans; extra thanks is due to Matthew Probert and Matt Segall. We would also like to thank NATO for a grant which has supported this work in part, the EPSRC (U.K.) E7 Grand Challenge in Colloidal Hydrodynamics for providing access to the Cray T3D at the Edinburgh Parallel Computing Center, the CSAR service at the University of Manchester for access to their Cray T3E and SGI Origin2000 through the EPSRC High Performance Computing for Complex Fluids Grant No. GR/M56234, and the Cambridge High Performance Computing Facility for access to their Hitachi SR2201. K.E.N. gratefully acknowledges financial support from NSERC (Canada) and the ORS Awards Scheme (U.K.).

APPENDIX: HIGH-PERFORMANCE COMPUTING

In this appendix we provide a few comments regarding the running of DPD simulations on high-performance computers. We usually had easy access to single-processor workstations, with a large variety of types and speeds of processors. Multiprocessor machines allowing parallel execution of simulations are much less common and are more difficult to obtain access to, although they have become more common during this research project. We used both the Cray T3D of the Edinburgh Parallel Computing Center (EPCC) and the Hitachi SR2201 of the Cambridge High Performance Computing Facility (HPCF) for computing the results described in this paper; the former consisted of 512 processor nodes and the latter consists of 256 nodes.

The implementation of the dissipative particle dynamics algorithm is very similar to that of conventional molecular-dynamics algorithms [55]. For example, we divide the periodic spatial domain (the simulation cell) into a regular array of equally sized link cells, such that each side of the rectangular domain has an integer number of cells and each cell is at least r_c across. Each link cell consists of a dynamically allocated array of particles and pointers to the neighboring cells. Individual particles consist of the position-momentum vector pair and a color index.

For each time step we iterate through the particles in each link cell, calculating the force acting on each particle as it interacts with the particles in the same and neighboring link cells. Since the DPD force acts between pairs of particles, we must ignore half of the neighboring cells to avoid duplication. When considering a different particle pair, we compare the square of the separation distance with r_c^2, skipping to the next particles if the pair is out of range. We then compute the new position and velocity as determined by the finite-difference algorithm [see Eq. (13) and Ref. [4]].

We may write the complete state of the system to file, and we can perform other calculations thereafter, for example to determine the temperature and pressure of the system. We used the freely available GNU-MAKE utility to dictate the compilation process, since the decision structures it contains make it simple to write programs portable to a large range of architectures. We created a comprehensive, automated test suite to make it easy to verify that optimizations of the calculations did not accidentally change the results of the computations.

Given constant r_c and number density $n = \rho/m$, the DPD algorithm scales linearly (in both computation time and

TABLE VIII. Elapsed time (in seconds) per node and parallel efficiency of various computers for the first 1000 time steps of a 6400-particle simulation in two dimensions. These computers were used to calculate the results in this paper.

Machine	Number of nodes	Elapsed time per node	Parallel efficiency
DEC 3000/400 AXP (133 MHz Alpha EV4)	1	624	
Linux PC (350 MHz Intel Pentium II)	1	180	
SGI Indigo2 (195 MHz MIPS R10000)	1	200	
EPCC Cray T3D (512×150 MHz Alpha EV4)	1	1254	1.00
	2	575	1.09
	4	354	0.89
	8	251	0.62
	16	206	0.38
	32	214	0.18
HPCF Hitachi SR2201 (256×150 MHz HARP-1E)	1	1202	1.00
	2	634	0.95
	4	371	0.81
	8	255	0.59
	16	212	0.35
	32	243	0.15

memory size) with an increasing number of particles (N), and is limited by computation time on all but the smallest machines. The main simulations we performed for this paper consisted of 6400 particles, and it is on the parallel and serial performance of this size of simulation that we will make most of the following comments. Details of the performance of this size of simulation in two dimensions are shown in Tables VIII and IX. These tables give the elapsed time per node in seconds and relative parallel efficiency for the first 1000 time steps, including data for a variety of computers and partition sizes. These data are for code compiled with the highest level of optimization, including some small reductions in floating-point accuracy. Table VIII describes the computers used to calculate the results in this paper, while Table IX describes the computers to which we have recently been allowed access, such as the Computer Services for Academic Research (CSAR) Cray T3E and SGI Origin2000 in Manchester.

A typical simulation of 50 000 time steps takes 2.5 h on a 350 MHz Intel Pentium II PC, the fastest single-processor machine to which we had common access. This same simulation would take 2.9 h on a 16-node partition of the T3D at the EPCC. However, to minimize fragmentation of the machine, jobs using up to 32 nodes were limited to a total execution time of 30 min. One possibility was to break up the run into 30-min portions, but this introduces additional overhead and complications; however, new jobs start instantly because they need not be queued. A better option was to run jobs on a 64-node partition, task farming four 16-node

TABLE IX. Elapsed time (in seconds) per node and parallel efficiency of various computers for the first 1000 time steps of a 6400-particle simulation in two dimensions. These computers were not used to calculate the results in this paper.

Machine	Number of nodes	Elapsed time per node	Parallel efficiency
SGI Octane	1	152	1.00
(250 MHz MIPS R10000)	2	87	0.88
CSAR Cray T3E-1200E	1	143	1.00
(576×600 MHz Alpha EV5)	2	96	0.74
	4	75	0.48
	8	67	0.27
	16	70	0.13
CSAR SGI Origin2000	1	133	1.00
(16×250 MHz MIPS R10000)	2	81	0.83
	4	69	0.49
	8	60	0.28

jobs to run simultaneously. There was a 12-h limit to 64–512 node jobs (6 h during the week), but there was often a long wait in the queues. If the efficient usage of billed time was a significant concern, sixteen 2-node jobs would complete in 8.0 h. However, during the week this meant restarting halfway through and waiting in the queue again. Similar comments apply to the Hitachi SR2201, although its queues were limited to 8 h maximum. The extra administrative overheads involved and the billed usage means that we usually concentrated computation on the serial workstations. However, parallel execution becomes more attractive with larger simulations.

The parallel efficiency of DPD with 6400 particles is good only for a modest number of processor nodes. This is particularly true of the more modern parallel machines such as the Cray T3E and SGI Origin2000, which are proportion-ally faster in processing than communicating when compared with their older counterparts. Much better parallel efficiency has been observed with larger simulations. The Cray T3D shows an unusual increase in efficiency when going from a serial calculation to a 2-node parallel calculation with 6400 particles; this could be explained by any number of hardware-specific arguments. We should note that the results for the Origin2000 include the effect of sharing the machine with other users, unlike all the other machines whose results appear in Tables VIII and IX, for which each node was dedicated to our calculations.

We decided to write the main simulation program in C/C++ as opposed to FORTRAN. This choice was made because C/C++ were believed to be the most appropriate languages for dealing with DPD simulations which consist of a large amount of bookkeeping wrapped around fairly simple computations. C/C++ and FORTRAN are highly portable to different computer architectures, and although well-written FORTRAN is more efficient on vector machines, for almost all other situations they are of similar speed, given equally good compilers. The use of vector machines (such as the Hitachi SR2201) was not anticipated when this work on DPD began several years ago. Furthermore, it was not believed that the basic algorithm would vectorize well, due to the short vector length in typical computations. Large programs are easier to maintain in C/C++ than in FORTRAN, although the increasingly well-supported FORTRAN 90 and 95 make the difference less significant.

Finally, we comment on our findings in tuning the message passing interface (MPI) calls for the Cray T3D. In our simulations, it was found that blocking calls (sends and receives) were faster than nonblocking calls and were easier to use correctly. Furthermore, better scaling was achieved by sending the size of a variable-size message in a separate message rather than probing incoming messages to determine their size. Finally, using derived data types to remove unneeded data from messages was slower than sending everything.

[1] P. V. Coveney and K. E. Novik, Phys. Rev. E **54**, 5134 (1996).

[2] P. V. Coveney and K. E. Novik, Phys. Rev. E **55**, 4831 (1997).

[3] K. E. Novik and P. V. Coveney, Int. J. Mod. Phys. C **8**, 909 (1997).

[4] K. E. Novik and P. V. Coveney, J. Chem. Phys. **109**, 7667 (1998).

[5] S. I. Jury, P. Bladon, S. Krishna, and M. E. Cates, Phys. Rev. E **59**, R2535 (1999).

[6] E. Velasco and S. Toxvaerd, Phys. Rev. Lett. **71**, 388 (1993).

[7] E. Velasco and S. Toxvaerd, J. Phys.: Condens. Matter **6**, A205 (1994).

[8] E. Velasco and S. Toxvaerd, Phys. Rev. E **54**, 605 (1996).

[9] M. Laradji, S. Toxvaerd, and O. G. Mouritsen, Phys. Rev. Lett. **77**, 2253 (1996).

[10] P. B. S. Kumar and M. Rao, Phys. Rev. Lett. **77**, 1067 (1996).

[11] A. Shinozaki and Y. Oono, Phys. Rev. Lett. **66**, 173 (1991).

[12] A. Shinozaki and Y. Oono, Phys. Rev. E **48**, 2622 (1993).

[13] J. E. Farrell and O. T. Valls, Phys. Rev. B **40**, 7027 (1989).

[14] O. T. Valls and J. E. Farrell, Phys. Rev. E **47**, R36 (1993).

[15] Y. Wu, F. J. Alexander, T. Lookman, and S. Chen, Phys. Rev. Lett. **74**, 3852 (1995).

[16] T. Lookman, Y. Wu, F. J. Alexander, and S. Chen, Phys. Rev. E **53**, 5513 (1996).

[17] F. Corberi, A. Coniglio, and M. Zannetti, Phys. Rev. E **51**, 5469 (1995).

[18] A. Chakrabarti, R. Toral, and J. D. Gunton, Phys. Rev. B **39**, 4386 (1989).

[19] A. Chakrabarti, R. Toral, and J. D. Gunton, Phys. Rev. E **47**, 3025 (1993).

[20] D. H. Rothman and J. M. Keller, J. Stat. Phys. **52**, 1119 (1988).

[21] D. H. Rothman, Phys. Rev. Lett. **65**, 3305 (1990).

[22] D. H. Rothman and S. Zaleski, Rev. Mod. Phys. **66**, 1417 (1994).

[23] S. Bastea and J. L. Lebowitz, Phys. Rev. E **52**, 3821 (1995).

[24] C. Appert, J. F. Olson, D. H. Rothman, and S. Zaleski, J. Stat. Phys. **81**, 181 (1995).

[25] A. N. Emerton, P. V. Coveney, and B. M. Boghosian, Phys. Rev. E **55**, 708 (1997).

[26] A. N. Emerton, P. V. Coveney, and B. M. Boghosian, Phys. Rev. E **56**, 1286 (1997).

[27] F. W. J. Weig, P. V. Coveney, and B. M. Boghosian, Phys. Rev. E **56**, 6877 (1997).

[28] F. J. Alexander, S. Chen, and D. W. Grunau, Phys. Rev. B **48**, 634 (1993).

[29] S. Chen and T. Lookman, J. Stat. Phys. **81**, 223 (1995).

[30] W. R. Osborn, E. Orlandini, M. R. Swift, J. M. Yeomans, and J. R. Banavar, Phys. Rev. Lett. **75**, 4031 (1995).

[31] E. Orlandini, G. Gonnella, and J. M. Yeomans, Physica A **240**, 277 (1997).

[32] G. Gonnella, E. Orlandini, and J. M. Yeomans, Phys. Rev. Lett. **78**, 1695 (1997).

[33] G. Gonnella, E. Orlandini, and J. M. Yeomans, Phys. Rev. E **58**, 480 (1998).

[34] A. J. Wagner and J. M. Yeomans, Phys. Rev. Lett. **80**, 1429 (1998).

[35] D. Sappelt and J. Jäckle, Europhys. Lett. **37**, 13 (1997).

[36] P. J. Hoogerbrugge and J. M. V. A. Koelman, Europhys. Lett. **19**, 155 (1992).

[37] P. Español and P. Warren, Europhys. Lett. **30**, 191 (1995).

[38] P. Español, Phys. Rev. E **53**, 1572 (1996).

[39] P. Español, M. Serrano, and I. Zúñiga, Int. J. Mod. Phys. C **8**, 899 (1997).

[40] R. D. Groot and P. B. Warren, J. Chem. Phys. **107**, 4423 (1997).

[41] C. W. Gardiner, *Handbook of Stochastic Methods* (Springer, Berlin, 1983).

[42] H. Risken, *The Fokker-Planck Equation: Methods of Solution and Applications*, 2nd ed. (Springer, Berlin, 1989).

[43] P. Español, Phys. Rev. E **52**, 1734 (1995).

[44] P. V. Coveney and P. Español, J. Phys. A **30**, 779 (1997).

[45] E. G. Flekkøy and P. V. Coveney, Phys. Rev. Lett. **83**, 1775 (1999).

[46] E. G. Flekkøy and P. V. Coveney (unpublished).

[47] A. J. Bray, Adv. Phys. **43**, 357 (1994).

[48] S. Bastea and J. L. Lebowitz, Phys. Rev. Lett. **75**, 3776 (1995).

[49] E. D. Siggia, Phys. Rev. A **20**, 595 (1979).

[50] P. Fratzl and O. Penrose, Phys. Rev. B **50**, 3477 (1994).

[51] H. Tanaka and T. Araki, Phys. Rev. Lett. **81**, 389 (1998).

[52] V. M. Kendon, J.-C. Desplat, P. Bladon, and M. E. Cates, Phys. Rev. Lett. **83**, 576 (1999).

[53] M. Grant and K. R. Elder, Phys. Rev. Lett. **82**, 14 (1999).

[54] L. D. Landau and E. M. Lifshitz, *Fluid Mechanics*, Vol. 6 of *Course of Theoretical Physics* (Pergamon Press, Oxford, 1959).

[55] M. P. Allen and D. J. Tildesley, *Computer Simulation of Liquids* (Clarendon, Oxford, 1987).

[56] P. A. Egelstaff, *An Introduction to the Liquid State* (Clarendon, Oxford, 1992).

[57] *Numerical Recipes in C: The Art of Scientific Computing*, edited by W. H. Press, S. A. Teukolsky, W. T. Vetterling, and B. P. Flannery, 2nd ed. (Cambridge University Press, Cambridge, 1992).

[58] M. U. A. Bromba and H. Ziegler, Anal. Chem. **53**, 1583 (1981).

[59] C. A. Marsh, G. Backx, and M. H. Ernst, Phys. Rev. E **56**, 1676 (1997).

[60] C. Marsh, Ph.D. thesis, University of Oxford (1998).

[61] M. R. Swift, W. R. Osborn, and J. M. Yeomans, Phys. Rev. Lett. **75**, 830 (1995).